

The Origin of Non-Thermal Emission from FSRQs

S. Gasparyan

ICRANet-Armenia, Marshall Baghramian Avenue 24a, Yerevan 0019, Republic of Armenia

Abstract

The observations of astrophysical sources in a large frequency range (from radio to very high energy gamma-ray bands) provide complete information on the non-thermal processes taking place in different objects. Here, the origin of broadband emission from the jets of flat-spectrum radio quasars are discussed. For the current study the blazars detected above 100 GeV: PKS 1441+25, 3C 279, PKS 1222+216, PKS 1510-089, as well as CTA 102, which was in flaring state in optical/UV, X-ray and high energy gamma-ray bands, are selected. The publicly available data of Fermi LAT, Swift UVOT/XRT, Nustar telescopes have been analyzed, which enables to identify the prominent flaring and quiescent states for those sources, as well as, study the spectral properties, constrain the size and location of the emitting region.

The multiwavelength emission spectra of those sources, in different states, are modelled, which is crucial for understanding the particle acceleration and emission processes in their jets. For this purpose, a new code that can derive the model free parameters which statistically better describe the observed data is used. It derives the best-fit parameters and their uncertainties through Markov Chain Monte Carlo sampling of the likelihood distributions. By means of the detailed theoretical modeling of acquired data, it was possible to derive or at least constrain some crucial parameters such as the magnetic field, jet energetics, electron energy density etc.

Keywords: *FSRQs, relativistic jets, gamma-rays, non-thermal emission, theoretical modeling*

1. Introduction

Understanding the formation, structure and evolution of our Universe is one of the greatest mysteries. The emission processes taking place in Galactic sources (e.g. pulsars, supernova remnants, binary systems etc.) are relatively well examined and are always among the most discussed topics in astrophysics, however, the recent major progress in the telescope technique makes it possible to investigate the physical processes in extragalactic objects as well. Among extragalactic sources, the most powerful γ -ray emitters are blazars, which are classified as a subclass of AGNs, whose jet makes small angle in respect to the observer (Urry and Padovani, 1995). Blazars are very strong non-thermal emitters in all observable energy bands, ranging from radio to γ -ray bands.

The extremely short and strong variability, as well as, strong polarization detected from those sources witness the extreme environments and undergoing processes in the jets of blazars, making the study of these objects one of the most important topics of modern astrophysics.

By observational properties, blazars are divided into BL-Lacertae (BL-Lac) and flat spectrum radio quasars (FSRQs). The latter, are low-peaked ($\nu_{peak} < 10^{14}$ Hz) blazars, and in average have decaying spectra in the MeV/GeV bands, which makes these objects less possible to detect in Very High Energy bands (VHE; > 100 GeV). Up to now, only seven of FSRQs have been detected in VHE γ -ray band, which makes these objects more interesting to investigate.

Now, with the available data, the evolution of the broadband emission from blazars can be followed in physically reasonable timescales. In the theoretical modeling of blazar emission two most actual problems are 1) identifying processes responsible for the time averaged emission from radio to HE/VHE γ -ray bands and 2) finding a model which can explain time evolution of SEDs that is physical connection between the emission in different states (flaring and quiescent). These are ambitious and very complicated problems but are the ultimate goals of any currently developing and proposed theories. In principle, these two problems are linked: in order to find a unique dynamical evolving radiative

model to explain the overall emission from blazars it is necessary to be able to explain the emission in different states which then can be generalized within one single emission scenario. In other words, in order to understand the global emission processes in the jet, initially the empirical models explaining the SEDs at any given period should be very well investigated. This will also provide most detailed information on the jet parameters and their evolution time which are necessary for developing a self-consistent radiation model.

Up to now various theories and models were proposed to explain the observed multiwavelength emission from blazars. Most of them were successful in explaining the multiwavelength spectra in a given period but usually they fail to model the SED observed in another period. This is normal since these models do not include physical connection between different states of the jet and are meant only to understand the emission observed at a given period. Moreover, sometimes the problems are even more complicated: two different models or the same model with another set of free parameters can equally well explain the observed data which introduces significant difficulties for theoretical modeling.

Since the main aim of the applied theoretical models is to gain as much as possible information from the observed spectra various statistical methods should be applied to compare different models or to find the set of free parameters which statistically better explain the observed data. The latter one is especially important as finding the parameters best explaining the data allows direct insight into the processes ongoing in the jet and constraining the parameters describing the jet. This implies that successful application of any theoretical model should also contain effective optimization of model free parameters. Since the models have nonlinear dependence from the model free parameters the effective optimization of the parameters is not a trivial task. There are various methods which can be used to find best description of the data one of the simplest one being calculation of chi-squares (χ^2) when the data and the models are compared. However, it is well known that the models with many free parameters are best optimized by Markov Chain Monte Carlo (MCMC) method. Due to the recent developments in high performance computing now the MCMC samplers with high number of steps can be used, so most precise results can be obtained.

Last but not least, the observations of blazars (especially in the γ -ray band) can help also to understand the formation of the Universe. The detection of distant γ -ray sources is restricted not only by their low emission flux (below telescopes sensitivities), but also the produced photons can be absorbed. They can interact with the photons of diffuse radiation in the Universe, so called extragalactic background light (EBL) and produce electron-positron pairs. The density of EBL photon field is composed by the light emitted since the formation of the Universe (stars, galaxies etc.) and it contains valuable information on the history of star and galaxy formation. The EBL density cannot be measured directly and it can be done only indirectly, namely when the γ -ray emission from a very distant blazar is observed, it can help to measure the limit of EBL photon density. Especially are important the observations of very distant blazars with Fermi LAT and ground based Cherenkov telescopes (MAGIC, VERITAS, HESS) so combining the data in the MeV/GeV (unabsorbed) and TeV (absorbed) bands can help to constrain the density of EBL. This once more emphasizes the importance of studying blazars in general and the origin of their emission in particular.

2. The study of blazar emission

2.1. Broadband emission from blazars

The electromagnetic emission from blazars is observed in a wide energy range from radio to HE γ -ray bands. This broadband emission is predominantly of a nonthermal origin, although, sometimes, thermal emission from some components can be also observed. The broadband SED of blazars has two nonthermal peaks - one at optical/UV or X-rays (the low-energy component) and the other at higher energies (the γ -ray band). The observed high-degree polarization indicates that the low-energy component is most likely due to the synchrotron emission of electrons accelerated in the jet. While the synchrotron emission can explain the observed features of the low-energy component, the origin of the HE component is still unclear, so various models/scenarios were proposed. One of the most widely applied models is that the HE component is produced via IC scattering of soft photons being either internal (e.g., synchrotron photons; SSC (Ghisellini et al., 1985) (Maraschi et al., 1992)) or external:

EIC (Sikora et al., 1994) (Ghisellini and Tavecchio, 2009) to the jet. The inverse Compton scattering of both internal and external photon fields are discussed in (Gasparyan, 2019). Discussed models are used in this study.

These pure leptonic models have been successful in explaining the SEDs of blazars but sometimes fail to reproduce some observed features. As a distinct alternative, models involving the radiative output of protons accelerated in the jet (hadronic models) were proposed (Mannheim and Biermann, 1992). The protons carry significant amount of energy and the exact estimation of their content in the jet can be crucial for understanding the physics of the jet. Even in the leptonic scenarios, hadrons (protons) are expected to be present in the jet to ensure the charge neutrality of the plasma. Then these protons can be effectively accelerated and by interacting with a dense target (proton-proton interaction), magnetic (proton-synchrotron) and/or photon fields ($p\gamma$ interaction) produce the observed HE component. In the case of hadronic models, more extreme parameters are required as compared with leptonic models (e.g., in the last two cases the protons should be accelerated beyond 10^{19} and propagate in a magnetic field exceeding 30 G (Mannheim and Biermann, 1992), (Mücke and Protheroe, 2001)) but in principle these conditions can be formed in the jet and sometimes the hadronic models give better modeling of SEDs (Böttcher et al., 2013). Leptonic one-zone emission scenarios are the most common models applied to explain the broadband emission from blazars. The emitting region is assumed to have a spherical geometry (blob) carrying a magnetic field with an intensity of B and a population of relativistic electrons/positrons. Since the emission region moves along the jet with a bulk Lorentz factor of Γ_{bulk} , the observed radiation will be amplified by a relativistic Doppler factor of $\delta = 1/\Gamma_{bulk}(1 - \beta \cos(\Theta_{obs}))$, where Θ_{obs} is the jet inclination angle (usually $< 8^\circ$ for blazars). The size of emission region can be constrained by the observed variability time-scale (τ), $R_b \leq \delta c \tau / (1 + z)$. It has already been noted that blazars are characterized by extreme variability (in both time and amplitude), which implies that the emission region should be very compact. For typical parameters of $t_{var} \sim$ few hours and $\delta \sim 10 \div 20$, the emission region cannot exceed 10^{15} - 10^{16} cm. This implies that blazar observations are unique tools for investigation of the sub-parsec structures of their jets. As the one-zone models assume the emission is produced from a single population of electrons, it is expected to have correlated flux changes in various bands (Ulrich et al., 1997). However, for some blazars the expected correlations were not observed, so alternative two-zone models were proposed (Kirk et al., 1998). The basic idea of two-zone models is that the multiwavelength emission is produced from two blobs having different size or location along the jet and each containing different population of particles. For example, one of these models assumes that particles are accelerated in one blob, but they emit whenever they are injected in the second blob. As an alternative, in order to explain the rapid variability in the γ -ray band, a model where the emission is produced in two emitting regions of different sizes and distances from the central source was proposed. Of course, two-zone models contain more free parameters, so are easier for modeling, but these are only possibilities, when complex changes of multiwavelength flux are observed. Now in the era of available large amount of multiwavelength data, not only currently known theories can be tested but also new emission models can be proposed.

2.2. Theoretical modeling of SEDs

The progress of theoretical astrophysics in understanding various processes allowed developing numerical simulation techniques to follow the jet from the beginning up to its termination point. For example, the impact of the jets on the environment where they propagate and their collimation and propagation can be investigated by realistic high-resolution simulations of the jets. By three-dimensional general relativistic magneto-hydrodynamic simulation of jet formation from an accretion disk allows to investigate their launching and acceleration. Of course, the simulations are a powerful tool for investigating different properties of the jet but they require initial parameters which can be obtained only from observations and theoretical modeling of the results. For example, the observations in radio band are unique to probe their morphology and the internal structures of the jet or the monitoring in HE γ -ray bands allows following the evolution of the system in time. On the other hand, the theoretical modeling of the broadband emission spectra will allow to estimate or at least constrain several important parameters, such as emitting particle energy density and distribution, magnetic field, etc., which are necessary to investigate the physics of the jets. Therefore, the high quality of the

observed multiwavelength data and their theoretical modeling has become one of the most actively discussed topics in modern astrophysics. As mentioned above, the modeling of multiwavelength spectra of blazars is a powerful method to investigate the physics of blazar jets. However, finding parameters of a model, which statistically best describe the observed data, is perhaps one of the most actual problems in the modeling the multiwavelength SEDs of blazars. There are two main methods of optimizing model free parameters: analytic (e.g. chi-square (χ^2) minimization, maximum log-likelihood estimation, etc.) and numerical (e.g. Newton's, steepest-descent, MCMC methods). Among analytical methods perhaps the simplest method defining the best fit of a function is the chi-square minimization, the idea of which is to minimize the difference between the observed data and prediction curve. Although, there are plethora of optimization techniques, for high-dimensional problems, containing many free parameters, more efficient, i.e. less expensive to compute, are numerical methods, among which one of most popular is MCMC method, which comprises a class of algorithms for sampling from a probability distribution and one can obtain a sample of the desired distribution by observing the chain after a number of steps. Running MCMC samplers allows finding the best-fit and uncertainties of the model free parameters. Due to the recent developments in high performance computing now the MCMC samplers with high number of steps can be used so most precise results can be obtained. In order to optimize the free parameters, when multiwavelength SEDs of blazars are modeled, a python code is developed. It is based on the Naima package (Zabalza, 2015), which is based on the emcee package, enables to constrain a model's free parameters by performing MCMC fitting. The MCMC approach, which is based on the Bayesian statistics, is superior to the grid approach with a more efficient sampling of the parameter space of interest, especially for high dimensions (Wraith et al., 2009). The algorithm behind the code is the affine-invariant ensemble sampling algorithm for MCMC method proposed by Goodman & Weare (Goodman and Weare, 2010), which has several advantages over traditional MCMC sampling methods (e.g. the Metropolis-Hastings algorithm) and excellent performance as measured by the autocorrelation time (Foreman-Mackey et al., 2013). The code derives the best-fit model and uncertainty distributions of spectral model parameters through MCMC sampling of their likelihood distributions. The code is used to study flaring activities in the jets of FSRQs.

3. The origin of flares

In the theoretical interpretation of the multiwavelength emission from blazars, the size/location of the emitting region, magnetic field and electron energy distribution are uncertain. Only during flaring periods some of the unknown parameters can be constrained based on the observations in different bands. The majority of the blazars detected in VHE γ -ray band are high-frequency-peaked BL Lacs for which the synchrotron bump is in the UV/X-ray bands. In addition to the BL Lacs, there are also 7 FSRQs detected in the VHE γ -ray band which is rather surprising, since the BLR structure of these objects, which is rich in optical-UV photons, makes these environments strongly opaque to VHE γ -rays (Liu and Bai, 2006) (Poutanen and Stern, 2010). Moreover, FSRQs have a relatively steep photon index in the energy range of >100 MeV as was observed with the Fermi LAT which does not make them as strong emitters of VHE γ -ray photons. Detection of FSRQs in the VHE γ -ray band is challenging for the near-black-hole dissipation scenarios; it assumes that the γ -rays are most likely produced farther from the central source, outside the BLR, where the dominant photon field is the IR emission from the dusty torus. Typically, the temperature of torus photons $\sim 10^3$ K is lower than that of the photons reflected in the BLR $\sim 10^5$ K, and, in principle, VHE photons with energy up to ~ 1 TeV can escape from the region. Thus, the observations of FSRQs in VHE γ -ray band provide an alternative view of blazar emission as compared to BL Lacs. Moreover, since FSRQs are more luminous than BL Lacs, they could, in principle, be observed at greater distances. Indeed, the farthest sources detected in the VHE γ -ray band are the FSRQs at a redshift of $z \geq 0.9$ (e.g., PKS 1441+25 (Abeysekara et al., 2015), (Ahnen et al., 2015) and S3 0218+35 (Ahnen et al., 2016)). That is why FSRQs are ideal for estimation of the intensity of EBL through the absorption of VHE photons when they interact with the EBL photons (Coppi and Aharonian, 1999), (Madau and Phinney, 1996).

3.1. High energy gamma-ray emission from PKS 1441+25

Among FSRQs, PKS 1441+25 is one of the most distant sources detected so far at $z = 0.939$ (Shaw et al., 2012). In April 2015 both VERITAS and MAGIC collaborations announced the detection of VHE γ -rays from PKS 1441+25 (with up to 250 GeV photons) (Mirzoyan, 2015), (Mukherjee, 2015). During the same period, the source had been also observed with the telescopes Swift and NuSTAR. The observations of PKS 1441+25 during the bright period in April 2015 by different instruments provide us with data on the maximums of the emitting components (Swift UVOT/ASAS-SN and Fermi LAT) as well as on the transition region between these components in the energy range from 0.3 to 30 keV (Swift XRT and NuSTAR) (Abeysekara et al., 2015). In order to scope and investigate the flaring periods, light curves with different equal time binning are generated (see in Fig. 1). Next, for detailed investigation of the flaring periods, the flux changes in time, a light curve has been generated by an adaptive binning method, where the time bin widths are flexible and chosen to produce bins with constant flux uncertainty (Lott et al., 2012). The light curves show a strong emission from the source detected on April 20 to 27, 2015. During the same period, the source had been also observed with the telescopes Swift and NuSTAR. Similar data (up to HE γ -ray band) are available also from the observations carried out on January 06 to 28, 2015, which is the period of the large flare that was observed with Fermi LAT. The source was in active state on 21-27 January, when on 24 January the flux increased up to $(2.22 \pm 0.38) \times 10^{-6}$ photon $\text{cm}^{-2} \text{s}^{-1}$. In April, when the source was detected in VHE band, the photon index in MeV/GeV energy range hardened and reached ≤ 1.9 most of the time, with the hardest photon index of $\Gamma = 1.54 \pm 0.16$, which is not typical for FSRQs. Moreover, the



Figure 1. The γ -ray light curve of PKS 1441+25 from January to December 2015 (a). The bin intervals correspond to 1-day (blue data) and 3-days (green data). The light curve obtained by adaptive binning method assuming 20 % of uncertainty is presented in red (b). The change of photon index for 3-day binning (green) and with adaptive binning method are shown in (c).

spectral analysis of Fermi LAT data reveal a deviation of spectrum from the simple power-law shape at $E_{\text{cut}} = 17.7 \pm 8.9$ GeV, which most probably is a result of electron cooling (Fig. 2). During the

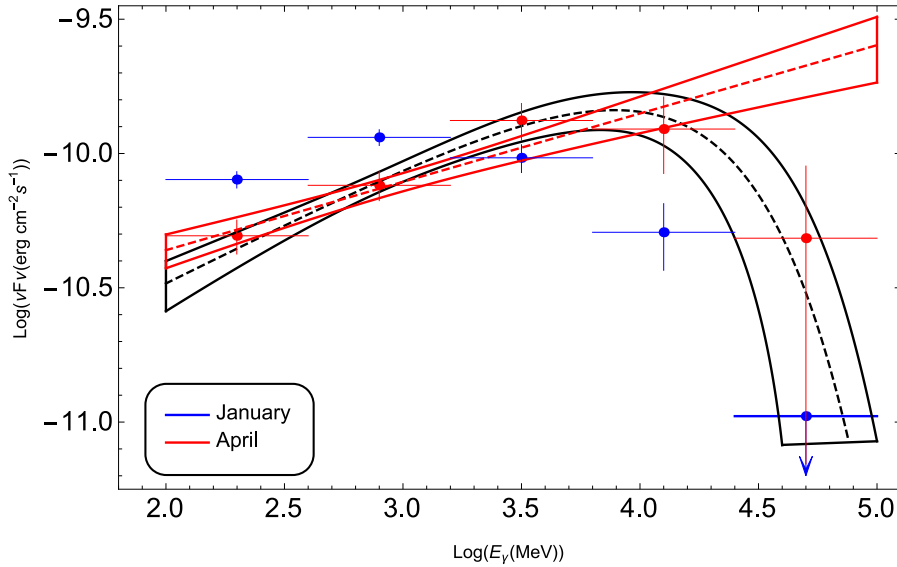


Figure 2. The γ -ray spectrum of PKS 1441+25 above 100 MeV averaged over the *Fermi* LAT observations in January (blue) and April (red).

January flare, the shortest flux variability is measured to be $\tau_d = 1.44$ days (see fig 2 in (Sahakyan and Gasparyan, 2017)), which enables to constrain the emitting region size up to $R_b \leq 3.5 \times 10^{16}(\delta/18)$ cm.

Actually, by modeling the emission in these two periods and estimating the parameter space that describes the underlying particle distribution responsible for the emission through MCMC technique, one can investigate and explore particle acceleration/ emission processes and jet properties in these two significant flaring periods which are crucial for understanding the origin of the flares. The broadband SEDs of PKS 1441+25 for different periods are shown in Fig. 3 where with red and blue colors are the SED observed in January and April respectively, while the archival data from ASI science data center are shown with gray color. We note that during the high states, the second emission peak increased by intensity and shifted to HEs. During the flaring periods the low-energy component's intensity increased as compared with the quiescent state; the increase in April exceeded that one observed in January (although the power-law photon index in the X-ray band (≈ 2.3) had been relatively constant during both observations). More evident and drastic is the change of the peak intensity of the low energy component; from January to April it increased by nearly an order of magnitude and as compared with the quiescent state it increased ≥ 15 times. On the contrary, the peak of the second component (in the HE γ -ray band) is relatively constant, only the photon index in the MeV-GeV energy range is harder during the observations in April. The Compton dominance of the source is stronger and evident during the flaring periods, which suggests that the density of the external photon fields significantly exceeds the synchrotron photon density ($U_{ext}/U_{syn} \gg 1$). Such a strong amplification of the emission from blazars can be explained by means of introducing changes in the emission region parameters (e.g. in the magnetic field, emitting region size, bulk Lorentz factor and others, and/or particle energy distribution). In principle, all the parameters describing the emitting region can be changed at the same time if the flares are due to a global change in the physical processes in the jet, which also affect the jet dynamics and properties. However, usually, the change in one or two parameters is enough to explain the flares. An interesting study of the flaring activity in FSRQs as a result of changes in different parameters has been investigated in (Paggi et al., 2011). Namely, the emission spectra evolution as a function of changes in different parameters (e.g., bulk Lorentz factor, magnetic field, accretion rate, etc.) is investigated. In the case of PKS 1441+25, during its flaring periods, both the low energy and HE components increased several times. The increase of the second component is most likely due to moving of the emitting region outside its BLR. In principle, there are two possibilities: i) either the emitting region moves faster due to increasing bulk Lorentz factor and leaves the BLR or ii) the bulk Lorentz factor is unchanged and only the emitting region is moving beyond the BLR.

In the first case, since the external photon density in the commoving frame of the jet depends on the Doppler boosting factor, a strong increase in the Compton dominance will be observed. Additional increase of the magnetic field from January to April is also evident when the low energy component kept increasing (this corresponds to the case shown in Fig. 1 (b) in (Paggi et al., 2011)). Accordingly, two possibilities are discussed. First, it is assumed that δ has increased from 10 in the quiescent to 18 in the flaring periods, and alternatively: the Doppler factor was constant ($\delta = 18$) in both periods. These values are below and above the estimated mean bulk Lorentz factor of FSRQs obtained from the analysis of a large sample of γ -ray emitting FSRQs (Ghisellini and Tavecchio, 2015). The emission region size can be estimated through the observed variability time scale $\tau = 1.44$ d implying that $R_b \leq \delta c\tau/(1+z) \approx 3.5 \times 10^{16}$ cm when $\delta = 18$ and $R_b = 1.92 \times 10^{16}$ cm when $\delta = 10$. The SEDs during quiescent and flaring states are modelled using one-zone leptonic models that include the synchrotron, SSC and external inverse Compton processes; the model parameters are estimated using the MCMC method. The underlying electron energy density is considered to have a broken power-law shape presented in (Sahakyan and Gasparyan, 2017).

The modelings with their estimated parameters are depicted in Fig. 3 and Table 1.

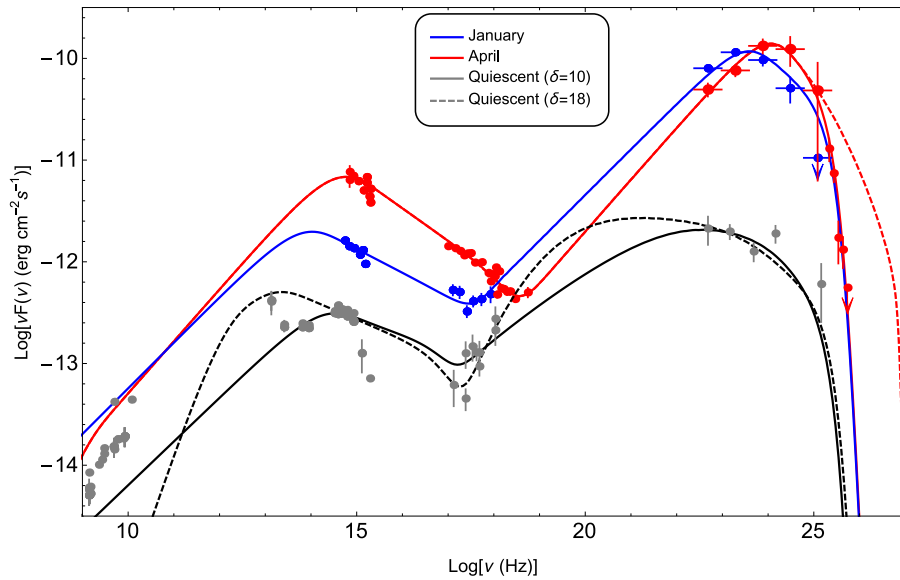


Figure 3. The broadband SED of PKS 1441+25 for January (red), April (blue) and for the quiescent state (gray). The model parameters are presented in Table 1. The UV-X-ray and VHE γ -ray data observed in January and April are from Abeysekera et al. (2015) and HE γ -ray data (Fermi LAT) are from this work.

The jet power in the form of magnetic field and electron kinetic energy are calculated by $L_B = \pi c R_b^2 \Gamma^2 U_B$ and $L_e = \pi c R_b^2 \Gamma^2 U_e$, respectively, and are given in Table 1. The jet power in the electrons changes in the range $(4.5 - 9.6) \times 10^{45}$ erg s^{-1} during the flares, while in the quiescent state it is of the order of $(2.1 - 4.1) \times 10^{45}$ erg s^{-1} .

The modelling shows that there is a hint of hardening of the low-energy index (~ 1.98) of the underlying non-thermal distribution of electrons responsible for the emission in 2015 April. Such hardening agrees with the γ -ray data, which pointed out a significant γ -ray photon index hardening on 2015 April 13 to 28. During the flaring periods, there are evident changes also in the underlying electron distribution. The electron distribution best describing the data observed in April hints at i) hardening of the low energy index, ii) a higher break at ~ 3.1 GeV and maximum energies of 203 GeV. E_{br} and E_{max} are expected to shift, as the γ -ray spectrum observed in April is slightly inclined toward HES, as compared with the January spectrum (see Fig. 3). Most probably these changes in spectrum caused the detection of this source in VHE γ -ray band.

More detailed interpretation of the obtained results can be found in (Sahakyan and Gasparyan, 2017).

Table 1. Model parameters.

	Parameter	Quiescent	Quiescent	January	April
Doppler factor	δ	10	18	18	18
Normalization of electron distribution	$N'_0 \times 10^{48} \text{ eV}^{-1}$	$10.68^{+3.09}_{-2.64}$	$43.44^{+6.59}_{-7.76}$	$23.83^{+8.11}_{-7.32}$	$6.12^{+1.67}_{-1.56}$
Low-energy electron spectral index	α_1	2.14 ± 0.04	$2.09^{+0.03}_{-0.04}$	$2.10^{+0.04}_{-0.05}$	1.98 ± 0.03
High-energy electron spectral index	α_2	$3.39^{+0.27}_{-0.14}$	3.38 ± 0.06	3.46 ± 0.06	3.64 ± 0.01
Minimum electron energy	E'_{\min} (MeV)	$1.84^{+1.75}_{-1.23}$	$286.37^{+30.64}_{-25.39}$	$1.97^{+0.31}_{-0.34}$	$4.16^{+1.00}_{-1.86}$
Break electron energy	E'_{br} (GeV)	$2.83^{+0.51}_{-0.31}$	$1.11^{+0.14}_{-0.12}$	$1.62^{+0.23}_{-0.15}$	$3.11^{+0.15}_{-0.23}$
Maximum electron energy	E'_{\max} (GeV)	$46.27^{+49.74}_{-13.76}$	$82.32^{+13.47}_{-17.14}$	$127.82^{+26.74}_{-24.75}$	$202.79^{+21.2}_{-14.6}$
Magnetic field	B [G]	0.19 ± 0.013	0.046 ± 0.002	$0.11^{+0.005}_{-0.004}$	$0.18^{+0.009}_{-0.006}$
Jet power in magnetic field	$L_B \times 10^{43} \text{ erg s}^{-1}$	0.49	0.31	1.71	4.51
Jet power in electrons	$L_e \times 10^{45} \text{ erg s}^{-1}$	2.11	4.07	9.60	4.47

3.2. More FSRQs on VHE γ -ray map

In order to understand the physical processes in the jets of FSRQs, the set of FSRQs have to be explored. Besides the PKS 1441+25 blazar, we initiated to model the SEDs in quiescent and different flaring states of PKS 1510-089, PKS 1222+216, 3C 279 FSRQs, which have been detected in VHE γ -ray band, as well.

PKS 1510-089 at a redshift $z = 0.361$ is a γ -ray bright quasar (H. E. S. S. Collaboration et al., 2013), (Aleksić et al., 2014). It is monitored in many energy bands, showing several bright periods with most rapid changes observed in the HE γ -ray band (the flux doubling timescale is as short as ~ 20 minutes (Foschini et al., 2013)). From many flares we selected these observed in March 2009 (Barnacka et al., 2014), in February-April 2012 (Aleksić et al., 2014), on 18 May 2015 (2015A) and on 22 May 2015 (2015B) which demonstrated interesting modification of the flux and photon index. The data in the quiescent state are time-averaged spectra from ASI science data center.

PKS 1222+216 has been active in the MeV/GeV band since September 2009 followed by brightening also in other observable wavebands. The source underwent two major flares with the maximum of $F_{(\gamma, > 100 \text{ MeV})} = 10^{-5} \text{ photon cm}^{-2} \text{ s}^{-1}$ in April and June 2010 (Tanaka et al., 2011). During the second flare the MAGIC telescope also observed increased γ -ray emission with a flux doubling timescale of ~ 10 min (Aleksić et al., 2011). The data for Flare 1 are from (Tavecchio et al., 2011), while for the quiescent state (collected from August 2008 to 12 September 2009) and Flare 2 are from (Lei and Wang, 2015).

3C 279 is probably one of the best and most studied blazar in the γ -ray sky. The emission from this blazar is variable in almost all observed frequencies. Sometimes the flares are simultaneous while in general different time lags are observed. In (Hayashida et al., 2012), analyzing multiwavelength light curves, they found at least 5 periods between 2008 and 2010 when the source was in the flaring state. Each of these flares is different (by means of the flux changes observed in different bands) and needs to be studied individually. For the current study we picked the Flare B (19 November- 9 December 2008) and G (30 July - 2 August 2009) from (Hayashida et al., 2012). During the first flare, the flux in the optical and γ -ray bands increased simultaneously, while the X-ray flux was relatively constant. On the contrary, during the second flare, the increase was observed in all bands (optical, X-ray and γ -ray). For the quiescent state the data collected from April to July 2010 are used (Paliya et al., 2015).

In Fig. 4 the multiwavelength SEDs of PKS 1510-089, PKS 1222+216 and 3C 279 are shown in the quiescent and flaring states. The observed fast variability indicates that their emission regions are compact but their localization is an open problem. Along the jet, the emission can be produced in different zones, and depending on the distance from the central black hole different components can contribute to the observed emission (Sikora et al., 2009).

The strong amplification of the emission from blazars can be explained by means of introducing

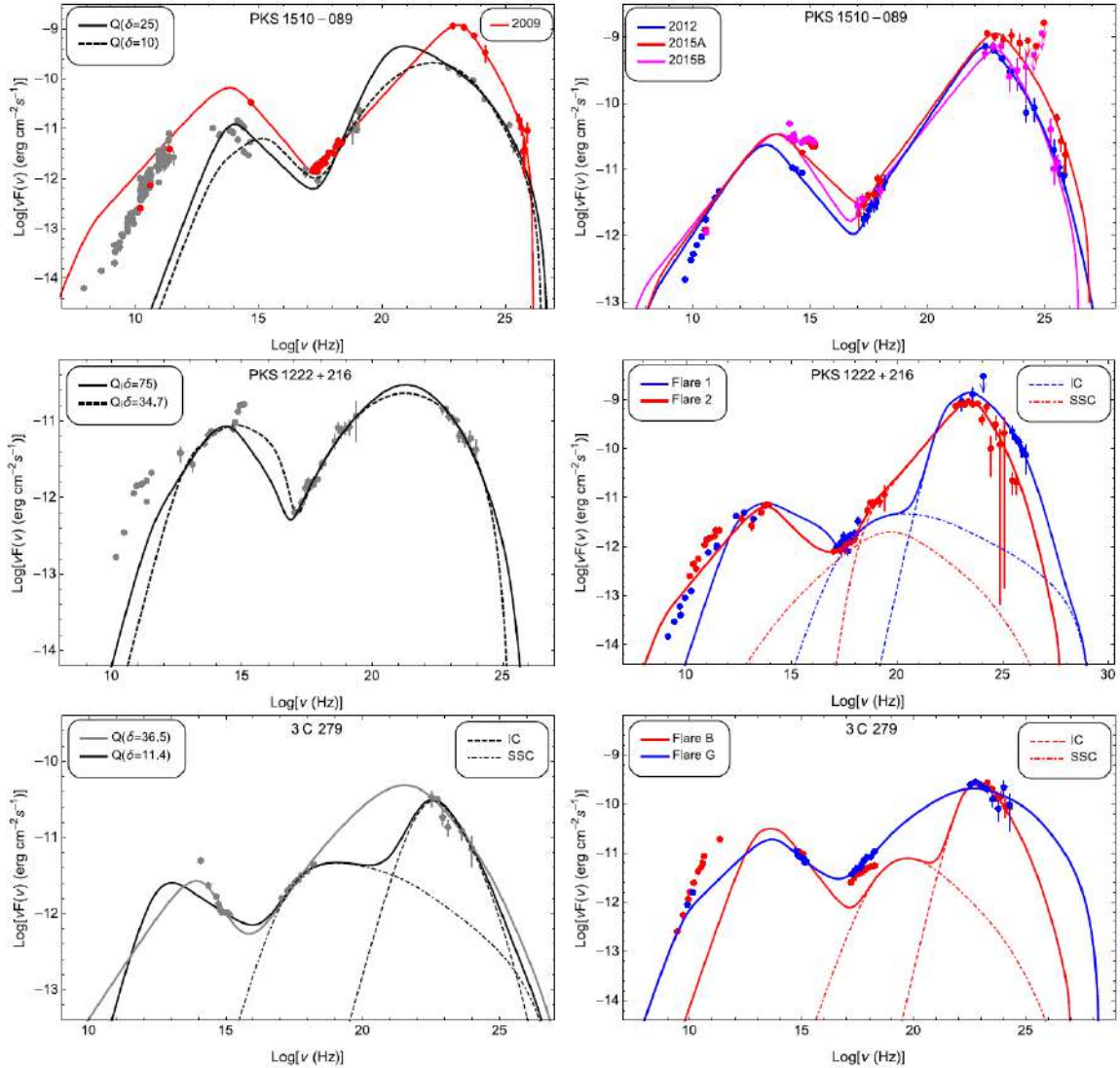


Figure 4. The broadband SEDs of blazars in the flaring and quiescent states. When EBL absorption is significant, the model and data are corrected for EBL absorption.

changes in the emission region parameters (e.g., in the magnetic field, emitting region size, bulk Lorentz factor and others, and/or particle energy distribution). We initiated to explain the flares with the change in one or two parameters is enough to explain the flares. During the flaring periods considered here both the low-energy and HE components are increased but the modification of HE emission component is more drastic. The increase of the second component is most likely due to moving of the emitting region outside the BLR. In the modeling of broadband SEDs we discuss two possibilities. First, we assume that δ has increased from the quiescent to the flaring periods (the values are given in Table 2), and then we assume that it was constant.

The results of the SEDs modeling are shown in Fig. 4 with the corresponding parameters in Table 2 where along with the best fit values also the uncertainties in the parameter estimation are provided. The SEDs observed during quiescent and flaring states are modeled using one-zone leptonic synchrotron and IC models, taking into account the seed photons originating inside and outside of the jet. The energy spectrum of the population of electrons in the jet frame, which is responsible for the non-thermal emission, is assumed to have a broken power-law shape (Gasparyan et al., 2018a).

Let us discuss the obtained results for 3C 279 FSRQ as perhaps the most interesting and complex SEDs are observed for this source (lower panel in Fig. 4). In the quiescent state the tail of the synchrotron emission is defined by the optical data, implying that the peak of the low-energy (synchrotron) component should be $< 10^{14}$ Hz. The IC scattering of these synchrotron photons is in the

Table 2. The parameters derived from the modeling of the SEDs of blazars in the quiescent and flaring states. For the emitting region size the following parameters were considered: for PKS 1510-089- $R = 4 \times 10^{14}$ cm and $R = 10^{15}$ cm for the quiescent and flaring states respectively; for PKS 1222+216- $R = 4.6 \times 10^{14}$ cm and $R = 10^{15}$ cm for the quiescent and flaring states respectively; for 3C 279- $R = 3.4 \times 10^{15}$ cm, $R = 1.1 \times 10^{16}$ cm and $R = 5.8 \times 10^{17}$ cm for the quiescent, periods B and G respectively.

	α_1	α_2	E'_{\min}	E'_{br}	E'_{\max}	B	L_B	L_e
			MeV	GeV	GeV	G	$\times 10^{41}$ erg s $^{-1}$	$\times 10^{44}$ erg s $^{-1}$
PKS 1510-089								
Q ($\delta = 10$)	$2.17^{+0.34}_{-0.27}$	$4.01^{+0.10}_{-0.07}$	$262.59^{+34.74}_{-56.62}$	$0.60^{+0.09}_{-0.09}$	$30.16^{+7.68}_{-4.04}$	$7.89^{+2.26}_{-1.45}$	37.3	1.67
Q ($\delta = 25$)	$1.83^{+0.05}_{-0.04}$	$3.96^{+0.02}_{-0.02}$	$514.92^{+9.94}_{-3.21}$	$0.58^{+0.02}_{-0.02}$	$90.75^{+4.48}_{-4.20}$	$0.37^{+0.01}_{-0.01}$	3.2	22
2009 ($\delta = 25$)	$1.91^{+0.01}_{-0.01}$	$4.13^{+0.20}_{-0.20}$	$0.77^{+0.02}_{-0.07}$	$0.63^{+0.01}_{-0.01}$	$25.77^{+0.59}_{-1.17}$	$0.45^{+0.01}_{-0.01}$	4.9	537
2012 ($\delta = 25$)	$1.93^{+0.03}_{-0.03}$	$3.84^{+0.03}_{-0.02}$	$0.93^{+0.21}_{-0.22}$	$0.296^{+0.009}_{-0.009}$	$74.87^{+42.11}_{-27.63}$	$0.357^{+0.002}_{-0.002}$	2.99	604.42
2015A ($\delta = 25$)	$2.02^{+0.10}_{-0.06}$	$3.68^{+0.08}_{-0.06}$	$1.27^{+0.80}_{-0.40}$	$0.46^{+0.08}_{-0.08}$	$139.88^{+120.62}_{-66.16}$	$0.34^{+0.01}_{-0.02}$	2.68	758.99
2015B ($\delta = 25$)	$2.11^{+0.04}_{-0.04}$	$4.04^{+0.12}_{-0.09}$	$0.61^{+0.11}_{-0.07}$	$0.52^{+0.07}_{-0.04}$	$54.71^{+23.66}_{-17.26}$	$0.46^{+0.02}_{-0.02}$	4.99	598.16
PKS 1222+216								
Q ($\delta = 34.7$)	$2.26^{+0.09}_{-0.07}$	$3.24^{+0.04}_{-0.04}$	$58.4^{+2.82}_{-3.01}$	$0.50^{+0.07}_{-0.04}$	$4.8^{+0.01}_{-0.01}$	$2.26^{+0.03}_{-0.03}$	49.8	3.2
Q ($\delta = 75$)	$1.86^{+0.02}_{-0.01}$	$3.93^{+0.06}_{-0.04}$	$38.90^{+1.79}_{-0.89}$	$1.07^{+0.04}_{-0.02}$	$11.13^{+0.06}_{-0.53}$	$0.162^{+0.003}_{-0.003}$	5.51	30.3
Flare1 ($\delta = 75$)	$2.24^{+0.42}_{-0.32}$	$3.41^{+0.16}_{-0.14}$	$60.07^{+13.12}_{-10.38}$	$0.31^{+0.07}_{-0.07}$	$13.16^{+2.34}_{-2.11}$	$0.42^{+0.03}_{-0.03}$	36.8	10.5
Flare2 ($\delta = 75$)	$1.959^{+0.005}_{-0.004}$	$3.91^{+0.01}_{-0.01}$	$1.04^{+0.03}_{-0.03}$	$0.334^{+0.005}_{-0.005}$	$294.75^{+28.33}_{-21.82}$	$0.473^{+0.002}_{-0.002}$	47.2	15.2
3C 279								
Q ($\delta = 11.4$)	$1.98^{+0.09}_{-0.13}$	$3.47^{+0.08}_{-0.03}$	$60.01^{+4.52}_{-4.53}$	$0.14^{+0.01}_{-0.01}$	$15.71^{+4.24}_{-3.88}$	$2.07^{+0.03}_{-0.06}$	242	3.7
Q ($\delta = 36.5$)	$1.91^{+0.01}_{-0.01}$	$4.28^{+0.04}_{-0.07}$	$4.77^{+4.29}_{-1.49}$	$2.86^{+0.07}_{-0.14}$	$469.41^{+34.04}_{-42.68}$	$0.0195^{+0.0009}_{-0.0003}$	2.26	285.73
Flare B ($\delta = 36.5$)	$2.598^{+0.307}_{-0.536}$	$4.17^{+0.43}_{-0.38}$	$129.76^{+38.79}_{-35.88}$	$0.48^{+0.11}_{-0.09}$	$121.51^{+94.66}_{-71.88}$	$0.56^{+0.06}_{-0.06}$	1872.7	9.3
Flare G ($\delta = 36.5$)	$2.10^{+0.05}_{-0.05}$	$3.74^{+0.03}_{-0.03}$	$121.10^{+31.10}_{-33.14}$	$11.72^{+1.01}_{-0.96}$	$2182.01^{+449.11}_{-238.69}$	$0.00056^{+0.00003}_{-0.00003}$	32.04	4801.56

Klein-Nishina regime ($\sim \gamma \nu_{syn}$), which means that it can explain the observed γ -ray data only if high δ is assumed. Thus, we assume two possibilities: when $\delta = 11.4$ is considered, the emission is explained by SSC, plus an additional contribution from BLR photons, instead, when $\delta = 36.5$, the emission in both X- and γ -ray bands are from IC scattering of synchrotron photons. In both cases, α_1 does not change significantly: $\alpha_1 = 1.98 \pm 0.11$ and $\alpha_1 = 1.91 \pm 0.01$ for $\delta = 11.4$ and $\delta = 36.5$, respectively. The break energy is higher when $\delta=36.5$ is used ($E'_{br} = (2.86 \pm 0.11)$ GeV versus $E'_{br} = (0.14 \pm 0.01)$ GeV), since the average energy of synchrotron photons is lower than that of BLR photons. When SSC+BLR model is used, the data can be explained for the jet with a total luminosity of $L_{jet} = 3.9 \times 10^{44}$ erg s $^{-1}$, and both the electrons and the magnetic field are almost in equipartition $U_e/U_B = 15.3$. For only SSC model, $L_{jet} = 2.9 \times 10^{46}$ erg s $^{-1}$ and $U_e/U_B = 1.3 \times 10^5$. During the Flare B, the emission in both optical and γ -ray bands increased, but it was almost constant in the X-ray band. Accordingly, in the fit we assume that the X-rays are due to another component, and require that SSC emission from the electron population producing the radio to optical emission does not over predict the observed X-ray flux (low right panel in Fig. 4). HE emission is modeled by IC scattering of dusty torus photons on the electrons with the power-law indexes $\alpha_1 = 2.56 \pm 0.44$ and $\alpha_2 = 4.17 \pm 0.41$ changing at $E'_{br} \approx (0.48 \pm 0.10)$ GeV, and $L_{jet} = 1.1 \times 10^{45}$ erg s $^{-1}$. During the Flare G, due to the simultaneous increase observed in the optical, X-ray and γ -ray bands, we conclude that the same SSC component is responsible for the emission in these bands. The emitting region size is larger (in (Hayashida et al., 2012) it has been shown that the flux variation time is 15 days), so a lower magnetic field $B = (560 \pm 30)$ μ G is obtained which results in the change of other parameters, e.g., $E'_{br} = 11.72 \pm 0.98$ GeV. The X-ray data allows the precise estimate of α_1 to be 2.10 ± 0.05 , a value which is expected from strong shock acceleration theories. In the jet the particle energy strongly dominates over the magnetic field ($U_e/U_B > 10^5$) and the jet total luminosity is $L_{jet} = 4.8 \times 10^{47}$ erg s $^{-1}$.

The obtained results presented in Table 2 are interpreted in (Gasparyan et al., 2018a).

The obtained results allow to quantitatively evaluate the jet energetics, break energy in the underlying

electron distribution in different states, which is crucial for investigating the changes in the physical state of the jet which caused the flares. However, the parameters describing the underlying electron distribution below the break are poorly constrained, because the data describing the rising part of both low-energy and HE components are missing. It did not allow us to exactly identify the processes responsible for the acceleration of particles in the jet. In principle, a similar study for the periods identified by the X-ray data can provide a chance to investigate the dominant particle acceleration processes, if the X-ray spectra define the rising part of the HE component.

4. On the multi-wavelength Emission from CTA 102

The modeling of blazar SEDs in quiescent and flaring states enables to understand the physical processes responsible for the emission. However, considering only the seven FSRQs detected in VHE γ -ray band we are limited for detailed investigation of the emission processes. Since the data only for observation in short periods are available and sometimes they are not simultaneous. Therefore, studying the emission only from FSRQs detected in the VHE γ -ray band does not allow to investigate the radiative output of emitting region while it moves along the jet. In order to study the emission produced from different zones of the jet we investigated the emission from well know blazar CTA 102. This source was selected since it is continuously monitored in various energy bands which provides huge amount of data allowing to study not only temporal correlation of emission in various bands but also model SEDs with simultaneous data observed in various periods. CTA 102 is a distant HE γ -ray emitting blazar ($z = 1.037$) detected but due to its distant most likely it cannot be observed in the VHE γ -ray band due to EBL strong absorption. For this blazar the large amount of data in radio, optical, X-ray and γ -ray bands are available, which enable to investigate the physical processes in both quiescent and active states of the jet, as well as distinguish the emission regions along the jet in different active periods.

For the present study we use the publicly available Fermi LAT, Swift UVOT/ XRT, NuStar data acquired in the period 2016-2018 when large-amplitude flares of CTA 102 were observed(Fig. 5). In the γ -ray band, Fermi LAT observed several prominent flares that followed a harder-when-brighter behavior. The peak γ -ray flux above 100 MeV, $(3.55 \pm 0.55) \times 10^{-5}$ photon $\text{cm}^{-2} \text{s}^{-1}$ was observed on MJD 57,738.47 within 4.31 minutes, corresponds to an isotropic γ -ray luminosity of $L_\gamma = 3.25 \times 10^{50}$ erg s^{-1} , comparable to the highest values observed from blazars so far. The analyses of the Swift UVOT/XRT data show an increase in the UV/optical and X-ray bands that is contemporaneous with the bright γ -ray periods. The X-ray spectrum observed by Swift XRT and NuSTAR during the γ -ray flaring period is characterized by a hard photon index of ~ 1.30 . The shortest e-folding time was 4.08 ± 1.44 hr, suggesting a very compact emission region $R \leq \delta \times 2.16 \times 10^{14}$ cm (Gasparyan et al., 2018b). The SEDs of CTA 102 in several periods (having different properties in UV/optical, X-ray, and γ -ray bands) is modeled assuming a compact blob inside and outside the BLR.

Fig. 6 shows the broadband SEDs of CTA 102 in its low and active periods together with the archival radio to X-ray data (light gray) from ASI science data center. The WISE IR data are highlighted by red asterisk which are most probably due to the torus emission as the recent studies show that the detection rate of almost all γ -ray blazars was high in the WISE all-sky survey (Massaro and D'Abrusco, 2016). The comparison shows that during the considered periods the fluxes in the optical/X-ray and γ -ray bands exceed the averaged archival data: the increase is more significant in the optical/UV band. This increase in all bands is expected as the selected periods correspond to the pre-flaring, flaring and post flaring states, and the source shows different emission properties as compared with the averaged spectrum.

Period 1 (P1): MJD 57625.06-57625.39 when the source was in the bright γ -ray state coinciding with XRT observations (Obsid: 33509022 and 33509023, merged during the analyses).

Period (P2): MJD 57738.02-57738.08, bright γ -ray period coinciding with the Swift Obsid: 33509106.

Period 3 (P3): ≈ 3.1 hour period centered on MJD 57752.52, corresponding to a bright γ -ray state coinciding with Swift (Obsid: 33509112 and 88026001, merged) and NuSTAR observations.

Period 4 (P4): ≈ 8.06 hour period centered on MJD 57759.62, corresponding to the period when the highest X-ray flux was observed (Obsid: 33509115).

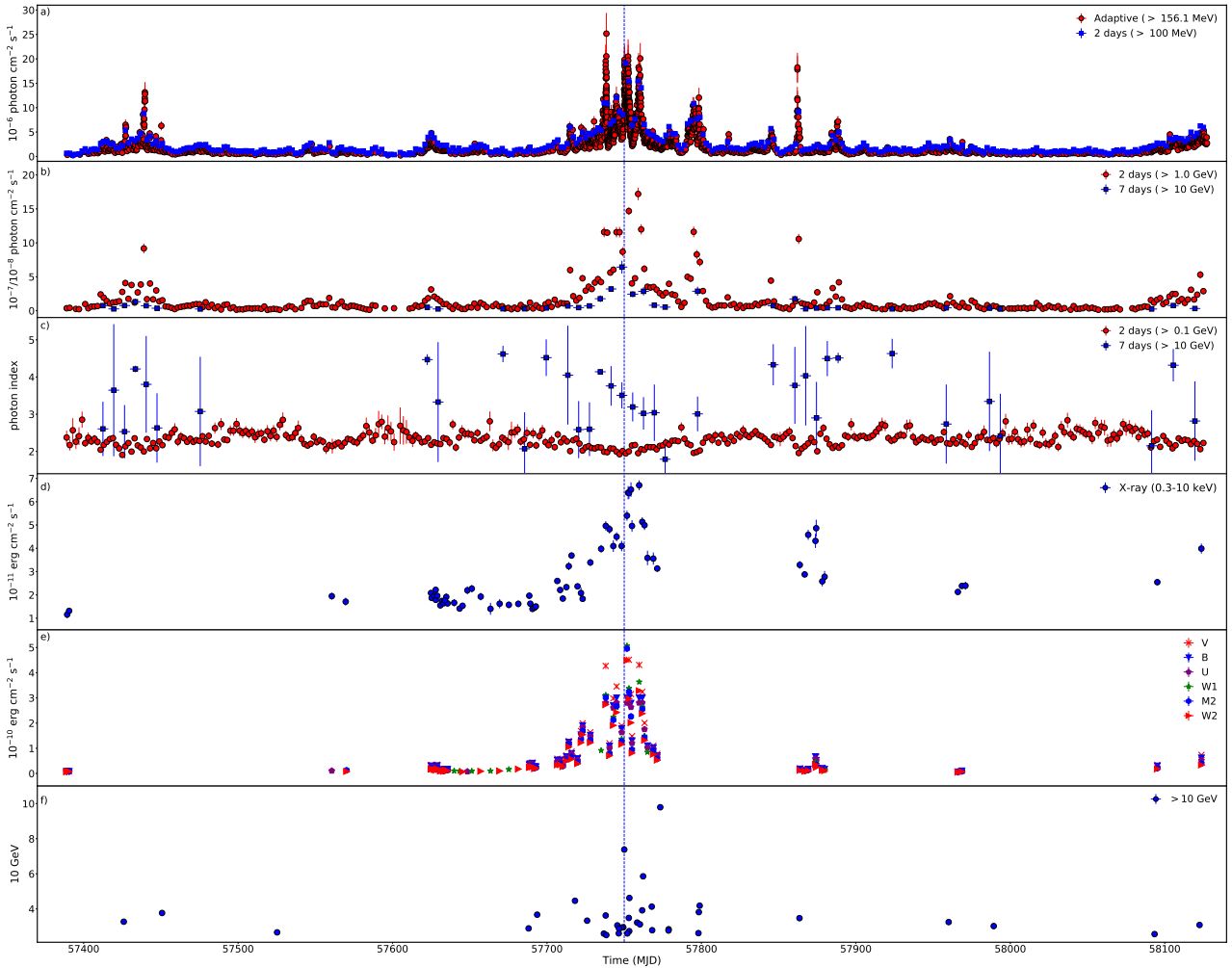


Figure 5. Multifrequency light curve of CTA 102 obtained for the period from 2008 August to 2018 January. *a)* γ -ray light curves with adaptive (red; ≥ 156.1 MeV) and 2-day (blue; 100 MeV) bins, *b)* and *c)* the flux and photon index with 2- and 7-days binning, *d)* Swift XRT light curve in the 0.3-10 keV range, *e)* UV/optical fluxes in *V*, *B*, *U*, *W1*, *M2* and *W2* bands and *f)* the energy and arrival times of the highest-energy photons. The vertical blue dashed line shows the period when a large flare in the *R*-band was observed (28 December 2016).

Period 5 (P5): ≈ 14.66 min period centered on MJD 57862.15, corresponding to another peak of γ -ray emission and available quasi-simultaneous Swift observation on the next day (Obsid: 33509121).

Comparing our selected periods i) the low-energy component increased while its peak frequency remained relatively constant ($\leq 10^{15}$ Hz), ii) the second component increased and shifted to HEs with a strong Compton peak dominance and iii) the UV/optical, X-ray and γ -ray fluxes contemporaneously increased in P2, P3 and P4, while the emission in the UV/optical and X-ray bands was relatively constant in P1 and P5.

The blazar flares can be explained by the changes in the magnetic field, in the emitting region size and its distance from the black hole, bulk Lorentz factor, particle energy distribution, etc. (Paggi et al., 2011). For example, both emission components will be shifted to HEs when the particles are effectively re-accelerated. Only the HE component will increase when the contribution of the external photon fields starts to dominate, for example, due to the changes in the location of the emitting region (Paggi et al., 2011). However, these are not unique models for explaining the flaring events. Another possibility is the geometrical interpretation of the origin of flares, the case when the jet regions may have different viewing angles. Such a model with a twisted inhomogeneous jet was already applied to explain the emission from CTA 102 jet in the optical, infrared and radio bands (Raiteri et al., 2017). The photons of different energy come from the jet regions which have different orientations (hence,

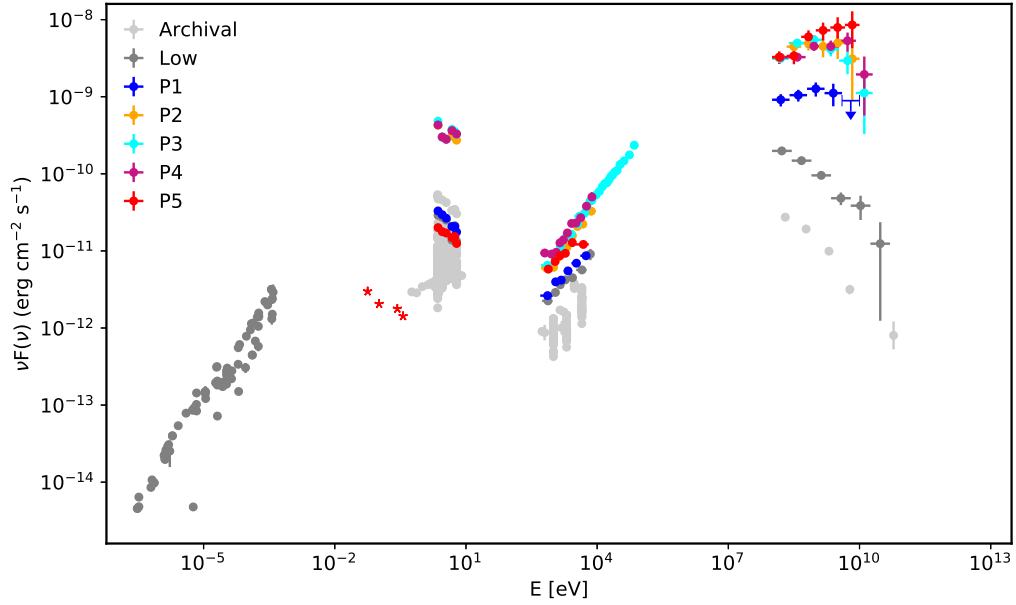


Figure 6. The broadband SEDs of CTA 102 in the selected periods. The archival data are shown in light gray.

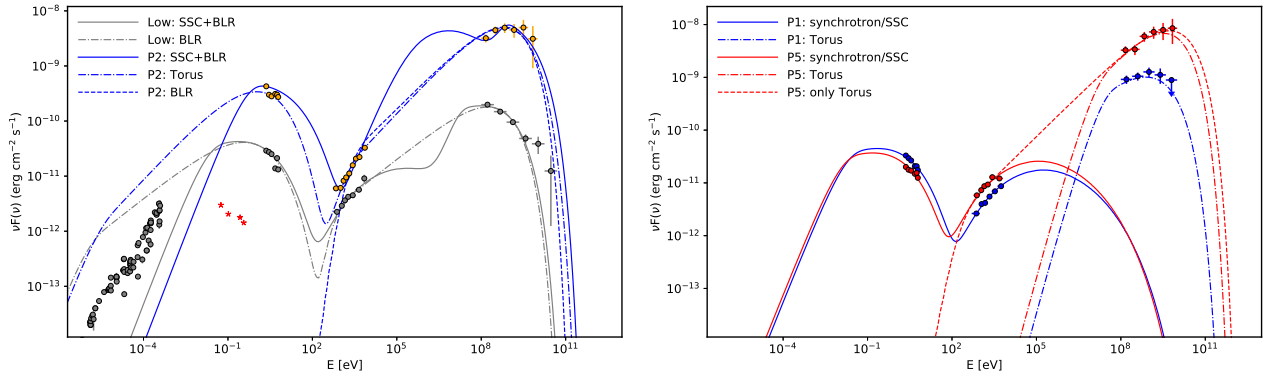


Figure 7. Modeling of the broadband SEDs of CTA 102 during the low state and P2 (left panel, gray and orange, respectively) and P1 and P5 (right panel, blue and red, respectively). The model parameters are given in Table 3. For the models applied see the text.

different Doppler boosting factors) because of the curvature of the jet.

The SEDs obtained in the low state, P1 and P5 showing different features, and in the bright P2 have been modeled. In order to account for Compton dominance, we assume the bulk Lorentz factor (δ which equals to the bulk Lorentz factor for small viewing angles, $\delta \approx \Gamma$) of the emitting region increased from 10 in the low to 20 in the active states (these are typical values estimated for FSRQs (Foschini et al., 2013)). In the modeling, the emission region is supposed to be filled by electrons having energy density of power-law with exponential shape (Gasparyan et al., 2018b).

When the SEDs in the low state and in P2 are modeled, the emission from a compact region inside and outside the BLR is discussed. Instead, when modeling the periods with lacking correlation in the γ -ray and UV/optical/X-ray bands, we assume the emission from the radio to X-rays is produced in the extended and slow-moving region unrelated to the flaring component, while the HE γ -rays come from a compact and fast-moving region outside BLR (Tavecchio et al., 2011).

Initially, we modeled the SED observed in the low state (Fig. 7; left panel). The radio data are treated as upper limits during the modeling, as the emission in this band is produced from the low-energy electrons which are perhaps from much extended regions. When the IC scatterings of both synchrotron and BLR photons are considered, the X-ray data allow to measure $E'_{min} = 68.25 \pm 5.27$

	Low		P1 Compact	P2		P5	
	SSC+BLR	BLR		SSC+BLR	Torus	Compact	Torus
δ	10	10	20	20	20	20	20
α	2.51 ± 0.11	2.19 ± 0.02	2.12 ± 0.54	2.79 ± 0.44	1.91 ± 0.03	1.78 ± 0.52	1.95 ± 0.03
E_{\min} (MeV)	68.25 ± 5.27	0.54 ± 0.03	155.59 ± 109.18	227.25 ± 26.43	1.38 ± 0.15	121.33 ± 67.33	0.63 ± 0.09
E_c (GeV)	0.67 ± 0.1	0.49 ± 0.04	1.42 ± 0.81	1.32 ± 0.43	0.98 ± 0.05	2.36 ± 1.54	3.85 ± 1.57
E_{\max} (TeV)	0.57 ± 0.31	0.49 ± 0.31	0.48 ± 0.34	0.50 ± 0.30	0.41 ± 0.18	0.58 ± 0.25	0.54 ± 0.31
B (G)	5.40 ± 0.13	5.37 ± 0.14	0.23 ± 0.29	6.10 ± 0.50	1.01 ± 0.003	0.004 ± 0.042	0.015 ± 0.049
L_B (erg s ⁻¹)	1.75×10^{46}	1.73×10^{46}	1.47×10^{42}	1.04×10^{45}	2.86×10^{43}	3.86×10^{38}	6.44×10^{39}
L_e [erg s ⁻¹]	4.66×10^{44}	2.90×10^{45}	1.73×10^{46}	2.84×10^{45}	2.74×10^{47}	7.33×10^{46}	1.97×10^{47}

Table 3. Parameters best describing the multiwavelength emission in different periods

MeV and $\alpha = 2.51 \pm 0.11$. In order to explain the observed UV/optical data, a $E'_c = 0.67 \pm 0.1$ GeV cut-off is required which makes the SSC component to decay in sub-MeV band and the HE data are described only by IC of BLR photons. Alternatively, both X-ray and γ -ray data can be described by IC scattering of BLR photons (dot-dashed gray line in Fig. 7) but the low-energy tail of IC spectra can reproduce the X-ray data only if $gamma_{min} = E_e/m_e c^2$ is close to unity (Celotti and Ghisellini, 2008). In this case, however, the synchrotron emission of these low energy electrons with $E_{min} = 0.54 \pm 0.03$ MeV will exceed the observed radio flux, making this scenario unlikely.

For the flaring states, it is found, that the HE data are better described when the infrared thermal radiation of the dusty torus is considered. In the flaring periods when the correlation between the γ -ray and UV/optical/X-ray bands is lacking, the γ -ray emission can be produced from the interaction of fresh electrons in a different blob, which does not make a dominant contribution at lower energies. The estimated values for flaring states are discussed and compared within each other in (Gasparyan et al., 2018b).

Consequently, some crucial parameters for the jet parameters were possible to constrain, for instance, the jet luminosity at different spatial regions along the jet, which can help to understand the effective γ -ray emission regions in the jets of FSRQs.

5. Conclusion

The origin of emission from FSRQ blazars which have been detected in VHE γ -ray band are studied. The ongoing physical processes in jets of these sources differ from the conventional the near-black-hole dissipation scenarios, making these objects interesting to investigate. In the study five FSRQs are included: four detected in VHE band, and one additional FSRQ, for which there are simultaneous large amount of data, which is crucial for not only probing the radiative processes in the jets but also identifying the effective γ -ray radiative zones within the jet. For these objects, the data from Fermi LAT, Swift UVOT/XRT and NuStar telescopes were collected/ analyzed, which enables to identify major activities/flares, study their properties and constrain the emission region size. The physical processes in the jets are studied by detailed investigation of their multiwavelength emission spectra. For that purpose, a python code is developed which in the optimization of model parameters uses MCMC methods. The modeling of the observed multiwavelength emission of blazar jets allows to estimate or put constraints on such important physical parameters of the jets as their composition, power, strength of magnetic field, electron energy distribution, etc., which are crucial for understanding of their physics. The obtained results are important and useful also for the future studies in the field.

References

- C. M. Urry and P. Padovani. Unified Schemes for Radio-Loud Active Galactic Nuclei. , 107:803, September 1995. doi: 10.1086/133630.
- G. Ghisellini, L. Maraschi, and A. Treves. Inhomogeneous synchrotron-self-Compton models and the problem of relativistic beaming of BL Lac objects. , 146:204–212, May 1985.
- L. Maraschi, G. Ghisellini, and A. Celotti. A jet model for the gamma-ray emitting blazar 3C 279. , 397:L5–L9, September 1992. doi: 10.1086/186531.
- M. Sikora, M. C. Begelman, and M. J. Rees. Comptonization of diffuse ambient radiation by a relativistic jet: The source of gamma rays from blazars? , 421:153–162, January 1994. doi: 10.1086/173633.
- G. Ghisellini and F. Tavecchio. Canonical high-power blazars. , 397:985–1002, August 2009. doi: 10.1111/j.1365-2966.2009.15007.x.
- S. Gasparyan. Modeling The Multiwavelength Spectra of Blazars. , 12(1):83–95, Feb 2019.
- K. Mannheim and P. L. Biermann. Gamma-ray flaring of 3C 279 : a proton-initiated cascade in the jet ? , 253:L21–L24, Jan 1992.
- A. Mücke and R. J. Protheroe. A proton synchrotron blazar model for flaring in Markarian 501. *Astroparticle Physics*, 15:121–136, March 2001. doi: 10.1016/S0927-6505(00)00141-9.
- M. Böttcher, A. Reimer, K. Sweeney, and A. Prakash. Leptonic and Hadronic Modeling of Fermi-detected Blazars. , 768(1):54, May 2013. doi: 10.1088/0004-637X/768/1/54.
- Marie-Helene Ulrich, Laura Maraschi, and C. Megan Urry. Variability of Active Galactic Nuclei. , 35:445–502, Jan 1997. doi: 10.1146/annurev.astro.35.1.445.
- J. G. Kirk, F. M. Rieger, and A. Mastichiadis. Particle acceleration and synchrotron emission in blazar jets. , 333:452–458, May 1998.
- V. Zabalza. naima: a python package for inference of relativistic particle energy distributions from observed nonthermal spectra. *Proc. of International Cosmic Ray Conference 2015*, page in press, 2015.
- Darren Wraith, Martin Kilbinger, Karim Benabed, Olivier Cappé, Jean-François Cardoso, Gersende Fort, Simon Prunet, and Christian P. Robert. Estimation of cosmological parameters using adaptive importance sampling. , 80(2):023507, Jul 2009. doi: 10.1103/PhysRevD.80.023507.
- Jonathan Goodman and Jonathan Weare. Ensemble samplers with affine invariance. *Communications in Applied Mathematics and Computational Science*, 5(1):65–80, Jan 2010. doi: 10.2140/camcos.2010.5.65.
- Daniel Foreman-Mackey, David W. Hogg, Dustin Lang, and Jonathan Goodman. emcee: The MCMC Hammer. , 125(925):306, Mar 2013. doi: 10.1086/670067.
- H. T. Liu and J. M. Bai. Absorption of 10-200 GeV Gamma Rays by Radiation from Broad-Line Regions in Blazars. , 653(2):1089–1097, Dec 2006. doi: 10.1086/509097.
- J. Poutanen and B. Stern. GeV Breaks in Blazars as a Result of Gamma-ray Absorption Within the Broad-line Region. , 717:L118–L121, July 2010. doi: 10.1088/2041-8205/717/2/L118.
- A. U. Abeysekara, S. Archambault, A. Archer, T. Aune, A. Barnacka, W. Benbow, R. Bird, J. Biteau, J. H. Buckley, V. Bugaev, J. V. Cardenzana, M. Cerruti, X. Chen, and et. al Christiansen. Gamma-Rays from the Quasar PKS 1441+25: Story of an Escape. , 815(2):L22, Dec 2015. doi: 10.1088/2041-8205/815/2/L22.

- M. L. Ahnen, S. Ansoldi, L. A. Antonelli, P. Antoranz, A. Babic, B. Banerjee, P. Bangale, U. Barres de Almeida, J. A. Barrio, W. Bednarek, and et al. Very High Energy γ -Rays from the Universe's Middle Age: Detection of the $z = 0.940$ Blazar PKS 1441+25 with MAGIC. , 815(2):L23, Dec 2015. doi: 10.1088/2041-8205/815/2/L23.
- M. L. Ahnen, S. Ansoldi, L. A. Antonelli, P. Antoranz, C. Arcaro, A. Babic, B. Banerjee, P. Bangale, U. Barres de Almeida, J. A. Barrio, J. Becerra González, W. Bednarek, E. Bernardini, A. Berti, B. Biasuzzi, and et.al Biland. Detection of very high energy gamma-ray emission from the gravitationally lensed blazar QSO B0218+357 with the MAGIC telescopes. , 595:A98, Nov 2016. doi: 10.1051/0004-6361/201629461.
- Paolo S. Coppi and Felix A. Aharonian. Simultaneous X-Ray and Gamma-Ray Observations of TEV Blazars: Testing Synchro-Compton Emission Models and Probing the Infrared Extragalactic Background. , 521(1):L33–L36, Aug 1999. doi: 10.1086/312168.
- Piero Madau and E. Sterl Phinney. Constraints on the Extragalactic Background Light from Gamma-Ray Observations of High-Redshift Quasars. , 456:124, Jan 1996. doi: 10.1086/176633.
- Michael S. Shaw, Roger W. Romani, Garret Cotter, Stephen E. Healey, Peter F. Michelson, Anthony C. S. Readhead, Joseph L. Richards, Walter Max-Moerbeck, Oliver G. King, and William J. Potter. Spectroscopy of Broad-line Blazars from 1LAC. , 748(1):49, Mar 2012. doi: 10.1088/0004-637X/748/1/49.
- R. Mirzoyan. Discovery of Very High Energy Gamma-Ray Emission from the distant FSRQ PKS 1441+25 with the MAGIC telescopes. *The Astronomer's Telegram*, 7416:1, Apr 2015.
- Reshmi Mukherjee. Very-high-energy gamma-ray emission from PKS 1441+25 detected with VERITAS. *The Astronomer's Telegram*, 7433:1, Apr 2015.
- B. Lott, L. Escande, S. Larsson, and J. Ballet. An adaptive-binning method for generating constant-uncertainty/constant-significance light curves with Fermi-LAT data. , 544:A6, August 2012. doi: 10.1051/0004-6361/201218873.
- N. Sahakyan and S. Gasparyan. High energy gamma-ray emission from PKS 1441+25. , 470:2861–2869, September 2017. doi: 10.1093/mnras/stx1402.
- A. Paggi, A. Cavaliere, V. Vittorini, F. D'Ammando, and M. Tavani. Flaring Patterns in Blazars. , 736:128, August 2011. doi: 10.1088/0004-637X/736/2/128.
- G. Ghisellini and F. Tavecchio. Fermi/LAT broad emission line blazars. , 448:1060–1077, April 2015. doi: 10.1093/mnras/stv055.
- H. E. S. S. Collaboration, A. Abramowski, F. Acero, F. Aharonian, A. G. Akhperjanian, G. Anton, S. Balenderan, A. Balzer, A. Barnacka, Y. Becherini, and et al. H.E.S.S. discovery of VHE γ -rays from the quasar PKS 1510-089. , 554:A107, Jun 2013. doi: 10.1051/0004-6361/201321135.
- J. Aleksić, S. Ansoldi, and et al. MAGIC gamma-ray and multi-frequency observations of flat spectrum radio quasar PKS 1510-089 in early 2012. , 569:A46, September 2014. doi: 10.1051/0004-6361/201423484.
- L. Foschini, G. Bonnoli, G. Ghisellini, G. Tagliaferri, F. Tavecchio, and A. Stamerra. Fermi/LAT detection of extraordinary variability in the gamma-ray emission of the blazar PKS 1510-089. , 555:A138, July 2013. doi: 10.1051/0004-6361/201321675.
- Anna Barnacka, Rafal Moderski, Bagmeet Behera, Pierre Brun, and Stefan Wagner. PKS 1510-089: a rare example of a flat spectrum radio quasar with a very high-energy emission. , 567:A113, Jul 2014. doi: 10.1051/0004-6361/201322205.

- Y. T. Tanaka, L. Stawarz, D. J. Thompson, F. D'Ammando, S. J. Fegan, B. Lott, D. L. Wood, C. C. Cheung, J. Finke, S. Buson, L. Escande, S. Saito, M. Ohno, T. Takahashi, D. Donato, J. Chiang, M. Giroletti, F. K. Schinzel, G. Iafate, F. Longo, and S. Ciprini. Fermi Large Area Telescope Detection of Bright γ -Ray Outbursts from the Peculiar Quasar 4C +21.35. , 733(1):19, May 2011. doi: 10.1088/0004-637X/733/1/19.
- J. Aleksić, L. A. Antonelli, and et al. MAGIC Discovery of Very High Energy Emission from the FSRQ PKS 1222+21. , 730:L8, March 2011. doi: 10.1088/2041-8205/730/1/L8.
- F. Tavecchio, J. Becerra-Gonzalez, G. Ghisellini, A. Stamerra, G. Bonnoli, L. Foschini, and L. Maraschi. On the origin of the γ -ray emission from the flaring blazar PKS 1222+216. , 534:A86, October 2011. doi: 10.1051/0004-6361/201117204.
- Maichang Lei and Jiancheng Wang. Location of gamma-ray flaring region in quasar 4C +21.35. , 67(4):79, Aug 2015. doi: 10.1093/pasj/psv055.
- M. Hayashida, G. M. Madejski, K. Nalewajko, M. Sikora, A. E. Wehrle, P. Ogle, W. Collmar, S. Larsson, Y. Fukazawa, R. Itoh, J. Chiang, L. Stawarz, R. D. Blandford, J. L. Richards, W. Max-Moerbeck, A. Readhead, R. Buehler, E. Cavazzuti, and et. al Ciprini. The Structure and Emission Model of the Relativistic Jet in the Quasar 3C 279 Inferred from Radio to High-energy γ -Ray Observations in 2008-2010. , 754(2):114, Aug 2012. doi: 10.1088/0004-637X/754/2/114.
- Vaidehi S. Paliya, S. Sahayanathan, and C. S. Stalin. Multi-Wavelength Observations of 3C 279 During the Extremely Bright Gamma-Ray Flare in 2014 March-April. , 803(1):15, Apr 2015. doi: 10.1088/0004-637X/803/1/15.
- M. Sikora, L. Stawarz, R. Moderski, K. Nalewajko, and G. M. Madejski. Constraining Emission Models of Luminous Blazar Sources. , 704:38–50, October 2009. doi: 10.1088/0004-637X/704/1/38.
- S. Gasparyan, N. Sahakyan, and P. Chardonnet. The origin of HE and VHE gamma-ray flares from FSRQs. *International Journal of Modern Physics D*, 27(10):1844007, Jan 2018a. doi: 10.1142/S0218271818440078.
- S. Gasparyan, N. Sahakyan, V. Baghmanyanyan, and D. Zargaryan. On the Multiwavelength Emission from CTA 102. , 863(2):114, Aug 2018b. doi: 10.3847/1538-4357/aad234.
- F. Massaro and R. D'Abrusco. The Infrared-Gamma-Ray Connection: A WISE View of the Extragalactic Gamma-Ray Sky. , 827:67, August 2016. doi: 10.3847/0004-637X/827/1/67.
- C. M. Raiteri, M. Villata, J. A. Acosta-Pulido, I. Agudo, A. A. Arkharov, R. Bachev, G. V. Baida, E. Benítez, G. A. Borman, W. Boschin, and et.al Bozhilov. Blazar spectral variability as explained by a twisted inhomogeneous jet. , 552:374–377, December 2017. doi: 10.1038/nature24623.
- A. Celotti and G. Ghisellini. The power of blazar jets. , 385:283–300, March 2008. doi: 10.1111/j.1365-2966.2007.12758.x.